Quasisteady and steady states in global gyrokinetic particle-in-cell simulations

S. Jolliet,[1] B. F. McMillan,[1] T. Vernay,[1] L. Villard,[1] A. Bottino,[2] and P. Angelino[3]
[1]*Association Euratom-Confédération Suisse, Centre de Recherches en Physique des Plasmas, Ecole Polytechnique Fédérale de Lausanne (EPFL), CH-1015 Lausanne, Switzerland*
[2]*Max-Planck-Institut für Plasmaphysik, Boltzmannstr. 2, D-85748 Garching, Germany*
[3]*Association Euratom CEA, CEA/DSM/IRFM, Cadarache, 13108 Saint-Paul-lez-Durance, France*

(Received 20 February 2009; accepted 30 April 2009; published online 26 May 2009)

Collisionless delta-*f* gyrokinetic particle-in-cell simulations suffer from the entropy paradox, in which the entropy grows linearly in time while low-order moments are saturated. As a consequence, these simulations do not reach a steady state and are unsuited to make quantitative predictions. A solution to this issue is the introduction of artificial dissipation. The notion of steady state in gyrokinetic simulations is studied by deriving an evolution equation for the fluctuation entropy and applying it to the global collisionless particle-in-cell code ORB5 [S. Jolliet *et al.*, Comput. Phys. Commun. **177**, 409 (2007)]. It is shown that a recently implemented noise-control algorithm [B. F. McMillan *et al.*, Phys. Plasmas **15**, 052308 (2008)] based on a W-stat provides the necessary dissipation to reach a steady state. The two interesting situations of decaying and driven turbulence are considered. In addition, it is shown that a separate heating algorithm, not based on a W-stat, does not lead to a statistical steady state. © *2009 American Institute of Physics*.
[DOI: 10.1063/1.3140036]

I. INTRODUCTION

Gyrokinetic simulations are presently the most advanced tools to study plasma turbulence,[1] which is commonly held responsible for the anomalous transport observed in experimental devices. A solid understanding of the characteristics and properties of turbulent transport is one of the main goals of gyrokinetic codes. Over the last decade, these codes have made several important discoveries including the stabilization of ion-temperature-gradient (ITG) turbulence by zonal flows.[2] Gyrokinetic codes can also provide an input for transport models[3] and several comparisons with experiments have recently been performed.[4,5] Regardless of the complexity of the implemented model, it is of course crucial for gyrokinetic codes to correctly describe the physics they contain. This can be checked by comparing the results with analytical theories[6] or with the help of code benchmarks.[7–9] The benchmarking exercise is quite difficult and the results of gyrokinetic codes have often been contradictory: Some of the best-known examples are very different heat transport levels found for electron temperature gradient (ETG) turbulence[10,11] and differing results for the role of the parallel nonlinearity[12,13] in ITG turbulence and the role of the zonal flows for trapped-electron-mode turbulence.[14,15] The observed differences are frequently attributed to the difference in numerical schemes between codes. The numerical methods to solve the gyrokinetic equations can be divided into three principle categories. In the Eulerian method,[16–20] the total or perturbed distribution function is stored on a five-dimensional (5D) grid and is evolved with spectral or finite difference methods. The main difficulties come from the Courant–Friedrich–Levy (CFL) condition and the convergence with respect to the grid size, which can be difficult to show. The semi-Lagrangian method[21–24] uses a fixed grid in time whereas the gyrokinetic equation is integrated along trajectories. This method removes the CFL condition but, as for Eulerian simulations, can lead to negative values of the distribution function. Finally, the particle-in-cell (PIC) method[2,25–30] samples the distribution function with numerical particles whose trajectory is evolved in time. This scheme is computationally less expensive than the Eulerian and semi-Lagrangian ones but suffers from statistical noise, which impairs the quality of the simulation and can even determine the final transport level, as shown in the case of ETG turbulence.[31]

Indeed, for δf PIC simulations, the noise problem is linked with another issue: Collisionless δf PIC simulations cannot achieve a steady state unless the system has some dissipation.[32] The fluctuation entropy, proportional to the sum of the weights squared $\langle w^2 \rangle$, grows together with the turbulence and one observes that low order moments saturate while the fluctuation entropy continually increases in time. Therefore, on top of the physical nonzero value of the fluctuation entropy there is a numerical growth of this quantity. This is known as the *entropy paradox* and is due to the Monte Carlo approach used in PIC codes. It means that δf collisionless PIC codes are not suited for performing long simulations and, therefore, their ability to make reliable quantitative predictions might be questioned. One way to resolve this entropy paradox is to introduce physical dissipation by implementing a collision operator. Unfortunately, this is a very difficult task in a 5D code: Collisions are usually implemented through a randomization of weights and/or velocities,[33] but this technique leads to a further increase in the numerical noise due to the weight spreading phenomenon.[34] The weights must be considered as an additional dimension in the system, which of course strongly increases the computational requirements. Various solutions

to this problem have been proposed such as a two-weight scheme[35] or a deterministic algorithm,[33] but due to the high computational requirements these methods have not been applied to a gyrokinetic 5D code so far.

Alternatively, one can remain collisionless and introduce numerical dissipation. Two examples are the particle-continuum method,[36,37] in which the weights and the phase space coordinates are periodically reset on a phase space grid, and the coarse-graining method,[38] in which the weights are binned on a 5D grid allowing the distribution function to be smoothed. Finally, a third method, originally proposed by Krommes,[32] consists of introducing a W-stat, which is a Krook-like dissipation term. This scheme is aimed at controlling the variance of weights and should therefore control the noise. A noise-control algorithm based on a W-stat (with the difference that the variance of the weights is not frozen to a given value) has been implemented[39] in the global collisionless gyrokinetic PIC code ORB5.[40] In Ref. 39, it is shown that the noise-control algorithm is able to stabilize the signal to noise ratio, meaning that one can run simulations up to arbitrarily long times, while recovering the collisionless limit of the ITG heat transport. In this paper, it is shown that ORB5 is able to reach a thermodynamical steady state through the noise-control algorithm presented in Ref. 39.

The remainder of this paper is organized as follows. In Sec. II, the gyrokinetic model and the ORB5 code are briefly introduced. Then, the evolution equation of the fluctuation entropy is derived and discussed in Sec. III. Simulation results are presented in Sec. IV. Finally, conclusions are exposed in Sec. V.

II. THE ORB5 CODE

The ORB5 code is described in details in Ref. 40; however the important points for the reader will be briefly summarized below. The code is global, i.e., profiles evolve self-consistently. Hahm's equations[41] are solved. In this paper we only consider the collisionless electrostatic limit with adiabatic electrons. The distribution function f is decomposed into an equilibrium Maxwellian $f_0(\hat{\psi},\epsilon,\mu)$ and a perturbed part $\delta f(\vec{z},t)$, where $\hat{\psi},\epsilon$ and μ are constants of the unperturbed motion, $\hat{\psi}$ is a constant of motion derived from the canonical angular momentum to avoid the generation of spurious zonal flows,[42] ϵ is the kinetic energy per mass unit, μ is the magnetic moment per mass unit $\vec{z}=(\vec{R},v_\parallel,\mu)$, $\vec{R}$ is the guiding center coordinate vector, and $v_\parallel$ is the velocity parallel to the magnetic field. The gyrokinetic equation reads

$$\frac{d\delta f}{dt} = \tau(\vec{E}) + S_K(\vec{z},t) + S_{\text{corr}}(\vec{z},t) + S_H(\epsilon,s,t), \tag{1}$$

$$\tau(\vec{E}) = -f_0\kappa(\hat{\psi})\left.\frac{d\hat{\psi}}{dt}\right|_1 + \frac{q_i f_0}{T_i}\langle\vec{E}\rangle\cdot\left.\frac{d\vec{R}}{dt}\right|_0, \tag{2}$$

where $s=\sqrt{\psi/\psi_{\text{edge}}}$ is a magnetic surface label, ψ is the poloidal magnetic flux, and $\tau(\vec{E})$ is the collisionless right-hand side of the Vlasov equation. The subscript 0 (respectively 1) denotes the unperturbed (respectively perturbed) motion $\kappa(\hat{\psi})=\partial \ln f_0/\partial\hat{\psi}$, q_i and T_i are the ion charge and temperature, and $\langle\vec{E}\rangle$ is the gyroaveraged electric field. $S_K(\vec{z},t)=-\gamma_K\delta f(\vec{z},t)$ is the Krook operator, where γ_K defines the amplitude of the artificial dissipation and is specified on the input. The Krook operator is further modified with the operator $S_{\text{corr}}(\vec{z},t)$ defined as

$$S_{\text{corr}}(\vec{z},t) = \sum_{i=1}^{N_{\text{mom}}} g_i(s,t) f_0(\hat{\psi},\epsilon,\mu) M_i(\vec{z}). \tag{3}$$

The $g_i(s,t)$ are determined in such a way that the Krook operator $S_K(\vec{z},t)+S_{\text{corr}}(\vec{z},t)$ does not modify an arbitrary set of N_{mom} moments. In practice, the set of moments includes the density $(M_1=1)$, the long time zonal flow structure $M_2=v_\parallel/B-\widetilde{v_\parallel/B}$ (see Ref. 6), where tilde denotes the bounce average and the kinetic energy per mass unit $M_3=1/2v^2$. If conservation of M_3 is enforced, the Krook operator will not introduce thermal energy into the system and the turbulence will decay. On the other hand, if it is not included then the Krook operator will heat the plasma. Nevertheless, the primary role of S_K is to control the noise and one would like to treat plasma heating independently. To this end, a heating operator $S_H(\vec{z},t)$ has been implemented, where

$$S_H(\epsilon,s,t) = -\gamma_H(s)\left(\breve{\delta f}(\epsilon,s,t) - \breve{f}_0(\epsilon,s)\frac{\int d\epsilon\breve{\delta f}(\epsilon,s,t)}{\int d\epsilon\breve{f}_0(\epsilon,s)}\right) \tag{4}$$

and $\gamma_H(s)$ is an input parameter. The breve symbol denotes an average over all the phase space dimensions except ϵ and s. In practice, the heating operator is obtained by building a (ϵ,s) binning of the markers. Unlike the Krook operator, the heating operator does not help control the noise because it does not act on the filamentation of the phase space in the $|v|$ direction (see Ref. 39 for more details). The second term of $S_H(\epsilon,s,t)$ is constructed such that the heating operator does not modify the density. A final important remark on the gyrokinetic equation is that formally ORB5 does not use a δf model for the Vlasov equation: The decomposition employed can be viewed as a "control variate" technique,[43] which is a numerical artifact and has no real physical meaning: f_0 is arbitrary, but its choice will of course affect the numerical noise in the simulation.

The quasineutrality equation is

$$\frac{en_0}{T_e}[\phi(\vec{x},t) - \bar{\phi}(\psi,t)] - \nabla_\perp\cdot\left[\frac{n_0}{B\Omega_i}\nabla_\perp\phi(\vec{x},t)\right] = \delta n_i(\vec{x},t), \tag{5}$$

where n_0 is the equilibrium density, T_e is the electron temperature, ϕ is the electrostatic potential, B is the strength of the magnetic field, Ω_i is the cyclotron frequency, δn_i is the perturbed density, and the bar is the flux-surface-average operator. This equation is solved with B-spline finite elements.[44,40] A particularity of ORB5 is that it does not use field-aligned coordinates but solves the quasineutrality equations on a (s,θ_*,φ) grid, where θ_* is the straight-field-line coordinate and φ is the toroidal angle. A field-aligned Fourier filter is then applied to the perturbed density: For a given set of toroidal modes, only the poloidal modes such that $|m$

$-nq(s)| < \Delta m$ are retained, where $q(s)$ is the safety factor profile and Δm is an input parameter. This procedure ensures that all modes of the simulation with small $k_\parallel / k_\perp$ are retained (of the order of $\rho^* = \rho_s / a$, where ρ_s is the ion sound gyroradius and a is the minor radius of the tokamak) consistently with the gyrokinetic ordering.[41] Moreover, the use of the field-aligned filter greatly decreases numerical noise by reducing the number of Fourier modes in the simulation.[45] A similar filter is applied to the left-hand side of the quasineutrality equation. The details of this solver will be published elsewhere. The field-aligned filter is also the starting point for the definition of a signal to noise ratio for ORB5 simulations (see Ref. 45). Modes outside the filter, which are generated mostly during the nonlinear phase of the simulation, do not satisfy the gyrokinetic ordering, and it is assumed that the amplitude in these modes is spuriously generated by noise due to Monte Carlo sampling. The mean squared amplitude in a certain band of these unphysical modes outside the filter is calculated: This is called the *noise*. The physical modes are the ones inside the field-aligned filter: The mean squared amplitude or the gyroaveraged density inside the filter is called the *signal*. The signal to noise ratio is simply the signal divided by the noise. This procedure is not able to extract the noise component of the mode inside the field-aligned filter. For this reason, this procedure is valid for high signal to noise ratios only. Note also that the $n=0$ toroidal mode is not incorporated in the signal: The noise accumulates in the undamped zonal flow component $m=0$, $n=0$ and it is not possible to extract separately the noise and the signal component. With ORB5, it is generally observed both for ETG (Ref. 45) and ITG (Ref. 39) turbulences that a signal to noise ratio above 10 is needed for convergence (in terms of heat transport). This threshold naturally depends on the choice of Δm and the band of Fourier modes used to calculate the noise. A simple formula for the noise can be computed,[45]

$$\delta n^2_{i,\mathrm{noise}}(t) \cong \frac{N_m}{N} \langle w^2 \rangle (t) G, \tag{6}$$

where N_m is the number of Fourier modes in the simulation, N is the number of markers, $\langle w^2 \rangle (t)$ is the sum of weights squared, and G is a constant that depends on the discretization algorithm used to solve the quasineutrality equation. This formula reveals that the important parameter in ORB5 is the number of markers per Fourier modes and not the number of markers per grid cell. This important statement is proved in Ref. 45.

The final important point to recall about ORB5 is that when the Krook and heating operators are turned off, a global particle and energy invariant can be analytically derived[46] and can be numerically checked (see Ref. 40 for examples). It is no longer the case when the noise-control algorithm is taken into account. Besides the convergence tests of the Krook operator performed in Ref. 39, a CYCLONE benchmark of ORB5 with other gyrokinetic codes has been published in Ref. 9.

III. THE FLUCTUATION ENTROPY BALANCE EQUATION

The fluctuation entropy, describing the difference between macroscopic and microscopic entropies, is defined according to Ref. 47,

$$\delta S = \int f(\vec{z},t) \ln[f(\vec{z},t)] - f_0(\hat{\psi},\epsilon,\mu) \ln[f_0(\hat{\psi},\epsilon,\mu)] d\vec{z}$$

$$\cong \frac{1}{2} \int \frac{\delta f^2(\vec{z},t)}{f_0(\hat{\psi},\epsilon,\mu)} d\vec{z}, \tag{7}$$

where the assumption $|\delta f| \ll |f_0|$ has been used. In the past, several studies on the fluctuation entropy have been made. An analytical study of the entropy production rate due to turbulence can be found in Ref. 48. Note that entropy production can also be studied in the frame of classical and neoclassical transports (see Ref. 49). Numerically, the fluctuation entropy has been studied with nondissipative Eulerian methods (both for collisionless[47] and collisional[50] cases) with the Eulerian code GYRO (Ref. 51) (where the dissipation comes from the upwind dissipation in radial and poloidal directions) in toroidal geometry and with the PIC code G4D (Ref. 52) in cylindrical geometry (without dissipation). Elsewhere, the growing weight problem has been solved by the coarse-graining algorithm,[38] which introduces dissipation and originates from the particle-continuum method.[37] In these papers the fluctuation entropy evolution equation is derived but is formally not studied numerically. In Ref. 38, the sum of weights squared is shown to be quasiconstant, indicating that a steady state was obtained. In what follows, the fluctuation entropy evolution equation is derived and numerically studied with the ORB5 code. First, the gyrokinetic equation, Eq. (1), is multiplied by $\delta f / f_0$ and integrated over the whole phase space,

$$\frac{d\delta S}{dt} = D_{\mathrm{flux}} + D_{\mathrm{field}} + D_{\mathrm{nc}} + D_{\mathrm{heat}}, \tag{8}$$

$$D_{\mathrm{flux}} = - \int d\vec{z} \left[\delta f + \frac{\delta f^2}{2 f_0} \right] \kappa(\hat{\psi}) \frac{d\hat{\psi}}{dt}, \tag{9}$$

$$D_{\mathrm{field}} = \int d\vec{z} \left[\delta f + \frac{\delta f^2}{2 f_0} \right] \frac{q_i}{T_i} \langle \vec{E} \rangle \cdot \frac{d\vec{R}}{dt}, \tag{10}$$

$$D_{\mathrm{nc}} = - \int d\vec{z} \gamma_K \frac{\delta f^2}{f_0} + \delta f \sum_{i=1}^{N_{\mathrm{mom}}} g_i M_i, \tag{11}$$

$$D_{\mathrm{heat}} = - \int d\vec{z} \gamma_H \left(\frac{\delta f \check{\delta} f}{f_0} - \frac{\delta f \check{f}_0}{f_0} \frac{\int d\epsilon \check{\delta} f}{\int d\epsilon \check{f}_0} \right). \tag{12}$$

Recall that Eq. (8) is valid for small $|\delta f|$ (compared to $|f|$). The evolution of the fluctuation entropy is caused by four different terms. D_{flux} describes the fluctuation entropy production by the profile gradients. It is instructive to see how D_{flux} relates to the heat diffusivity in the flux tube limit $\rho^* \to 0$ with constant profiles and gradients. By further assum-

ing circular geometry and by neglecting the term proportional to δf^2, one obtains

$$D_{\text{flux}} = \frac{a}{V}\left(\frac{a}{L_T}\right)^2 n_0 \chi_i, \tag{13}$$

where V is the plasma volume, L_T is the characteristic length of the ITG and χ_i, defined through $Q=-n\chi_i \nabla T \cdot \vec{e}_\psi$ with Q as the radial heat flux, and $\vec{e}_\psi$ is a unit vector in the ψ direction. This equation is similar to Eq. (52) of Ref. 51 and shows that D_{flux} is the driving term proportional to the heat diffusivity and responsible for the increase in the fluctuation entropy.

D_{field} describes the rate of fluctuation entropy created by the transfer of energy from the particles to the field perturbation. It can be shown that

$$D_{\text{field}} \cong -\frac{1}{T_i}\frac{dE_f}{dt}, \tag{14}$$

where the term proportional to δf^2 has also been neglected and E_f is the total field energy of the system, $E_f = q_i/2 \int d\vec{x} \delta n_i(\vec{x},t)\phi(\vec{x},t)$. This relation implies that when the electrostatic potential acquires energy, the entropy is reduced. This term should therefore be negative during the linear phase and then oscillate around 0 during the nonlinear phase.

D_{nc} (respectively D_{heat}) are the contributions from the noise-control (respectively heating) operators. It is shown in Appendix that D_{nc} and D_{heat} are always negative. However, it is expected that $|D_{\text{heat}}| \ll |D_{\text{nc}}|$ as the heating operator does not help in controlling the noise.

IV. SIMULATION RESULTS

A. Simulation parameters

The different terms of Eq. (8) have been implemented in ORB5 and studied for standard CYCLONE simulations[7] at $\rho^* = 1/184.7$. The physical parameters are $a=0.625$ [m], $B_0 = 1.91$ [T], $R_0=1.70$ [m], $\tilde{\rho}_0=0.5$, $q(\tilde{\rho}_0)=1.4$, $T_i=T_e$, $R_0/L_{Ti}=6.9$, $\eta_i=L_n/L_{Ti}=3.12$, and $\hat{s}(\tilde{\rho}_0)=0.78$. Here a is the minor radius of the tokamak, B_0 is the magnetic field on axis, R_0 is the major radius, $\tilde{\rho}_0$ is the reference normalized radius ρ_0/a in the plasma, q is the safety factor, L_{Ti} and L_n are the characteristic lengths of ion temperature and density, and $\hat{s}$ is the magnetic shear. A circular equilibrium is used with a safety factor profile given by $q(\tilde{\rho})=q_0+(q_{\text{edge}}-q_0)\tilde{\rho}^2$, where $\tilde{\rho}=\rho/a$, ρ is the radial coordinate, $q_0=0.85$, and $q_{\text{edge}}=3.04$. Numerical parameters are $N=80\times10^6$ markers, $\Delta t = 40\ \Omega_i^{-1}$. The quasineutrality equation is solved with cubic B-splines on a $N_s=128, N_{\theta_*}=512, N_\varphi=256$ grid and a field-aligned filtering is applied with $\Delta m=5$. The latter is combined with a rectangular filter $n_1=0\le|n|\le n_2=57$, $m_1=-128\le m\le m_2=128$. Poloidal modes above $k_\theta \rho_{Li}=1.0$ are filtered out. 80M markers correspond to ~5 markers per cell but correspond to ~700 markers per Fourier mode. The temperature profile is shown in Fig. 1. Five simulations have been performed requiring 2 days on a BG/L machine with 512 biprocessor nodes for each run. The first simulation has no Krook and no heating operators. The second one has no heating operator but a Krook operator with $\gamma_{Ki}=9\times10^{-5}\ \Omega_i$ with conserved density, zonal flow structure, and energy, i.e., the Krook operator allows temperature gradient relaxation. The third simulation is similar to the second one except that the conservation of energy is not imposed for the Krook operator: The Krook operator acts as heating. The fourth simulation has no Krook operator but the heating operator is turned on with $\gamma_H(s)=\gamma_H=9\times10^{-5}\ \Omega_i$. Finally the fifth simulation has both operators turned on with $\gamma_{Ki}=\gamma_H=9\times10^{-5}\ \Omega_i$ and the Krook operator conserves the energy. These simulations will be called transient, noise-controlled, fixed-gradient-noise-controlled, heated, and noise-controlled-heated. The values of γ_K and γ_H are roughly one tenth of the maximum linear growth rate in accordance with Ref. 39. Note that the choice of values of γ_K and γ_H does not change the conclusions. The convergence of the heat flux with γ_K and γ_H is discussed in Ref. 39.

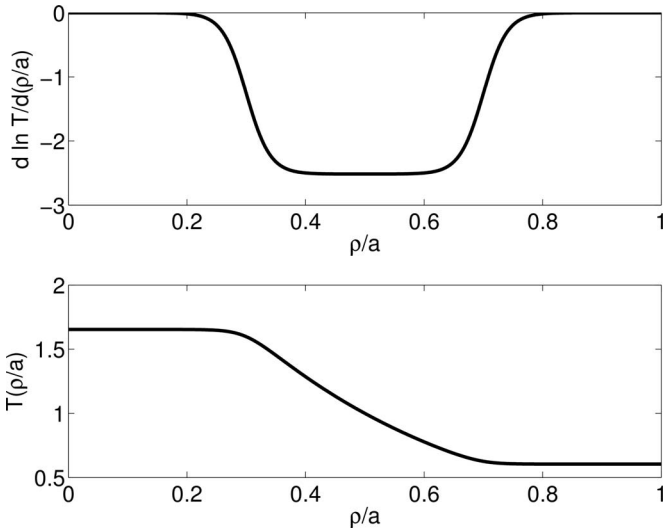

FIG. 1. Logarithmic temperature gradient and temperature profiles used in all simulations.

B. Results for decaying simulations

Figure 2 shows the different components of the fluctuation entropy evolution equation for the *transient* simulation. It exhibits a quasisteady state. In the end of the simulation, the entropy production rate is constant and almost equal to D_{flux}, while D_{field} is close to 0. This is the situation with saturated low-order moments and a growing entropy $\delta S \propto \chi_i t$. This simulation rapidly becomes dominated by numerical noise. As can be seen from Fig. 3, the signal to noise ratio is almost equal to 1 in the end of the simulation. According to Eq. (6), it is obvious that a quasisteady state will always be noisy as the noise is proportional to $\langle w^2 \rangle$, hence to $\delta S \sim \chi_i t$.

From Fig. 4, one sees the beneficial effect of D_{nc} on the entropy balance for the *noise-controlled* case. This term is always negative and balances D_{flux} (although the bursts of D_{nc} are slightly shifted in time with respect to those of D_{flux}). Like for the transient case, D_{field} is again extremely close to 0. Consequently, the noise-controlled simulation exhibits a steady-state character in the sense that in the end of the simulation, the fluctuation entropy is constant (see Fig. 5). This

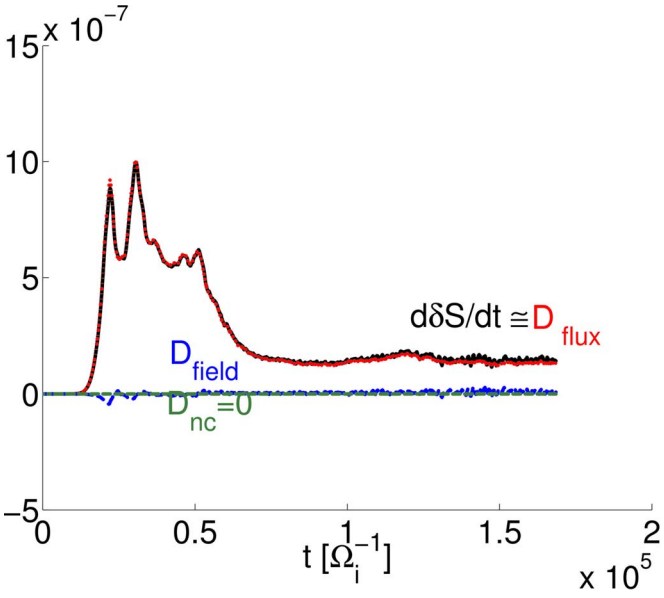

FIG. 2. (Color online) Temporal evolution of $d\delta S/dt$ (black solid line), D_{flux} (red dotted line), D_{field} (blue dashed line), and D_{nc} (green dashed-dotted line) for transient simulation. D_{heat} is zero.

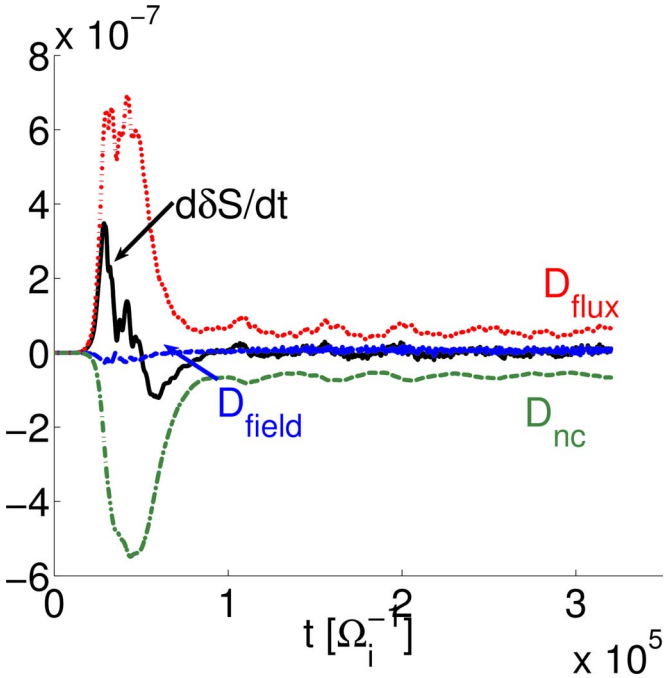

FIG. 4. (Color online) Temporal evolution of $d\delta S/dt$ (black solid line), D_{flux} (red dotted line), D_{field} (blue dashed line), and D_{nc} (green dashed-dotted line) for noise-controlled simulation. D_{heat} is zero.

proves that a W-stat allows for a true steady state. Note that the signal to noise level drops below 10 near $t=7\times10^4\ \Omega_i^{-1}$ and ends up at around 4, but the simulation seems to remain in a steady state. However, by looking more carefully at the noise-controlled fluctuation entropy evolution, Fig. 6, one sees that the fluctuation entropy slowly increases with time (from $\delta S=1.5\times10^{-3}$ at $t=1\times10^5\ \Omega_i^{-1}$ to $\delta S=2.15\times10^{-3}$ at $t=3.2\times10^5\ \Omega_i^{-1}$, i.e., a 30% increase). In this decaying simulation, the heat diffusivity goes to 0 as the temperature profile relaxes. It becomes more and more difficult to accurately represent this low signal with markers and the signal to noise ratio increases. The entropy production due to noise cannot be compensated by the dissipative Krook term anymore and so the fluctuation entropy increases: The system undergoes a transition from steady to quasisteady. This is better seen in Fig. 6. For 20M markers, the growth of the noise is larger and the Krook damping rate is clearly not large enough to counteract this effect, while the growth of the fluctuation entropy is smaller for 80M and 320M cases. Increasing the dissipation will delay this phenomenon but one must then be careful about physical convergence. The important conclusion is that decaying PIC simulations cannot be run for infinitely long times even when dissipation is introduced in the system. However one hopes to run them for the longest possible time in order to approach the critical

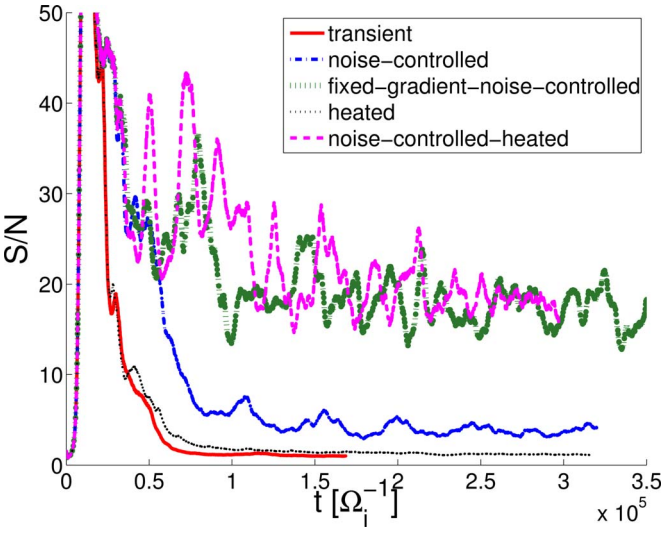

FIG. 3. (Color online) Temporal evolution of signal to noise ratio for transient (red solid line), noise-controlled (blue dashed-dotted line), fixed-gradient-noise-controlled (green dotted line), heated (black thin dotted line), and noise-controlled-heated (magenta dashed line) simulations.

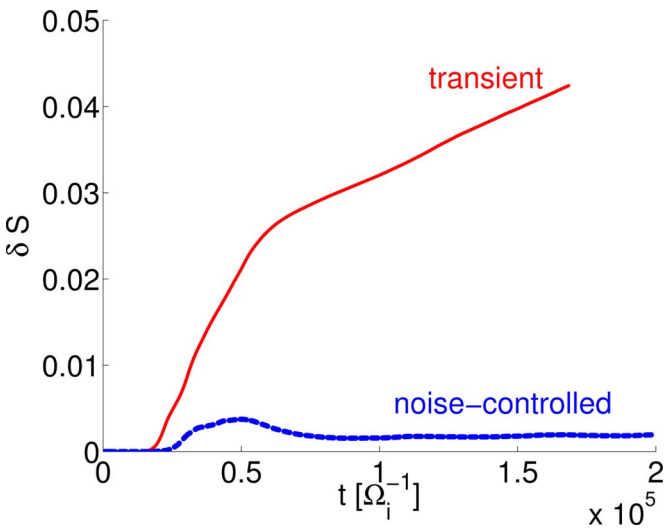

FIG. 5. (Color online) Temporal evolution of δS for transient (red solid line) and noise-controlled (blue dashed line) simulations.

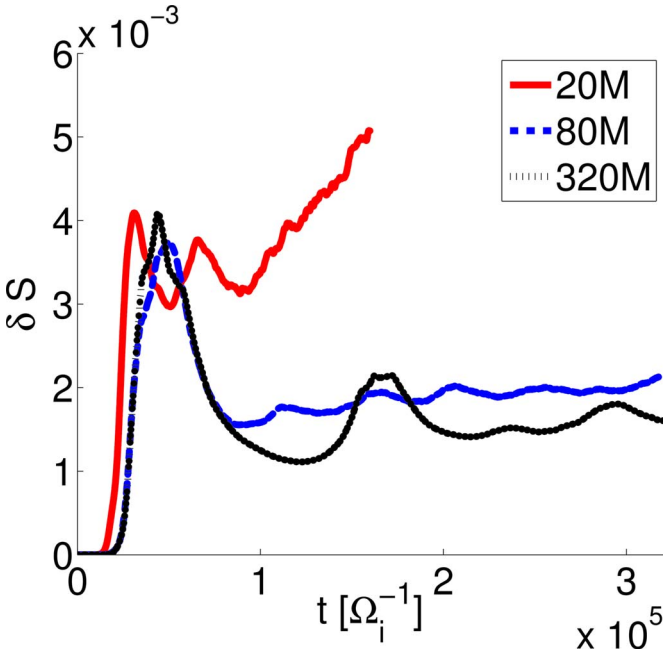

FIG. 6. (Color online) Temporal evolution of δS for noise-controlled simulations with 20M (red solid line), 80M (blue dashed line), and 320M (black dotted line) markers.

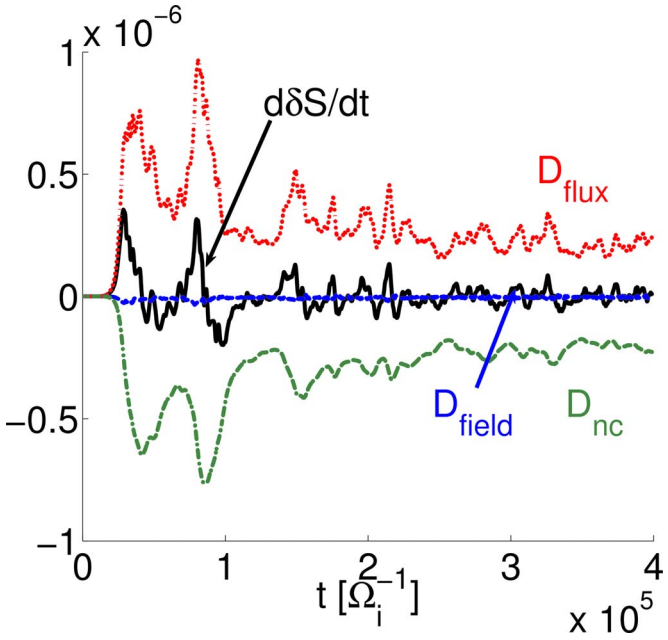

FIG. 8. (Color online) Temporal evolution of $d\delta S/dt$ (black solid line), D_{flux} (red dotted line), D_{field} (blue dashed line), and D_{nc} (green dashed-dotted line) for fixed-gradient-noise-controlled simulation. D_{heat} is zero.

gradient. In practice, the signal to noise ratio and the fluctuation entropy diagnostic provide a meaningful way to determine when the simulation becomes flawed and must be stopped. The number of markers and the dissipation can then be modified depending on how close is the final state of the system to the marginal point.

Figure 7 shows the time evolution of D_{flux} and χ_i/χ_{GB} (averaged between $\tilde{\rho}=0.3$ and $\tilde{\rho}=0.7$). The latter quantity has been rescaled by a constant factor to match the maximum value of D_{flux}. It is remarkable how these curves overlap despite the approximations made to obtain Eq. (13) and the fact that the heat diffusivity is radially averaged (one cannot average over the whole plasma because χ_i goes to infinity when ∇T goes to zero at the magnetic axis and at the plasma edge).

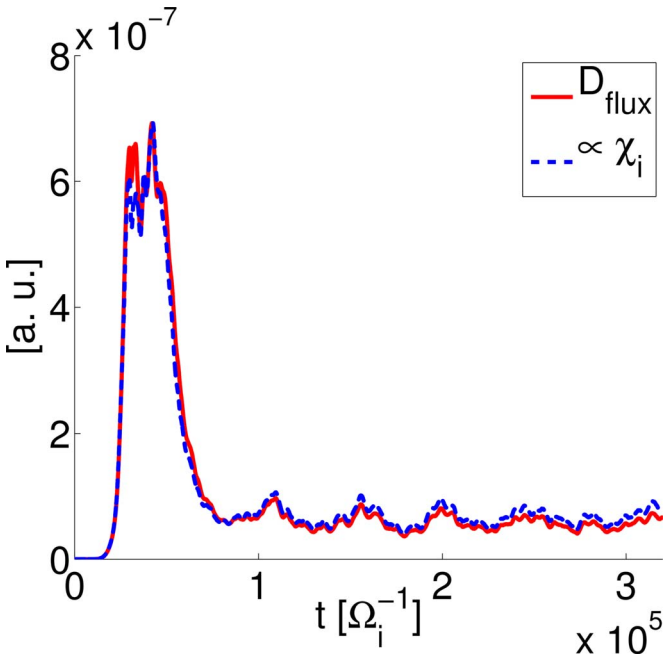

FIG. 7. (Color online) Time evolution of D_{flux} (red solid line) and χ_i/χ_{GB} (blue dashed line radially averaged between $\tilde{\rho}=0.3$ and $\tilde{\rho}=0.7$) for a noise-controlled simulation. χ_i/χ_{GB} has been rescaled by a constant factor to match the maximum of D_{flux}.

C. Results for driven simulations

Figure 8 displays the components of the fluctuation entropy equation for the *fixed-gradient-noise-controlled* simulation case. Because the gradient is kept almost fixed by the noise-control algorithm, the heat diffusivity and consequently the three components D_{flux}, D_{field}, and D_{nc} have a burstier character. Nevertheless, the entropy production rate approaches to 0 on time average and a true steady state is reached.

Finally, the influence of the heating operator on the fluctuation entropy is examined. In Figs. 9 and 10, the different components of the fluctuation entropy balance equation are represented for *heated* and *noise-controlled-heated* simulations. By looking at D_{heat}, one sees that this term, although slightly negative, is small and as expected does not significantly reduce the fluctuation entropy. Like the transient case, the heated case also exhibits a quasisteady state, where $\delta S \propto \chi_i t$. χ_i is much higher than its counterpart in the transient simulation reflecting the effect of heating, but the noise accumulates. The signal to noise ratios of transient and heated cases are very similar and are around 2 (see Fig. 3) which clearly demonstrates that these two simulations are noise dominated. This is why D_{flux} (and equivalently the heat transport) has some fast frequency oscillations and no burst activity. It must be emphasized that the average value of

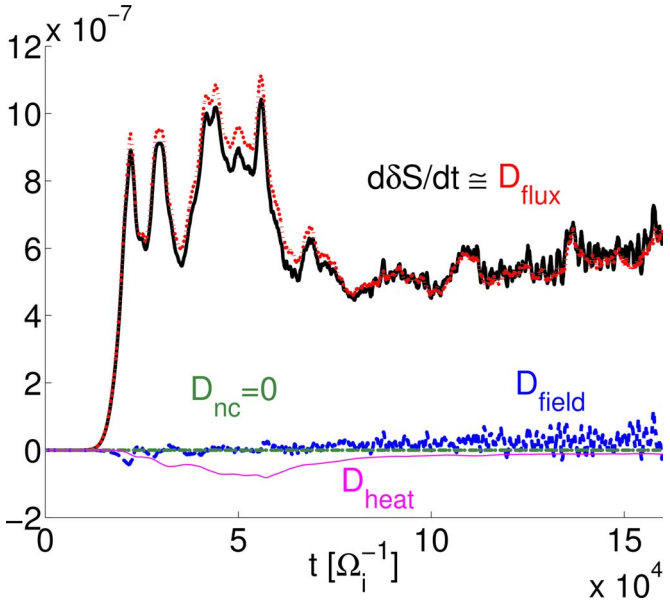

FIG. 9. (Color online) Temporal evolution of $d\delta S/dt$ (black solid thick line), D_{flux} (red dotted line), D_{field} (blue dashed line), D_{nc} (green dashed-dotted line), and D_{heat} (magenta thin solid line) for heated simulation.

D_{flux}, which is proportional to the average value of heat diffusivity, is in that case probably not converged.

The situation is fortunately much better in the noise-controlled-heated case, as can be observed from Fig. 10. D_{heat} is again very small and slightly negative, but here the noise-control component prevents the entropy from growing. On average, $d\delta S/dt$ is zero, demonstrating that the noise-controlled-heated case has reached a steady state. The most striking difference between the two simulations with heating is observed on D_{flux}. In the noise-controlled-heated case, the system undergoes an endless series of heat bursts while in the heated case the burst phenomena stop and are replaced by

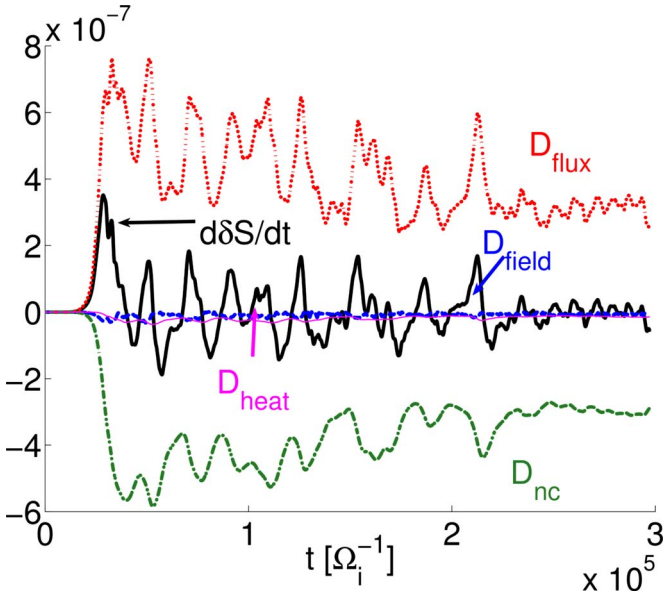

FIG. 10. (Color online) Temporal evolution of $d\delta S/dt$ (black solid thick line), D_{flux} (red dotted line), D_{field} (blue dashed line), D_{nc} (green dashed-dotted line), and D_{heat} (magenta thin solid line) for heated simulation.

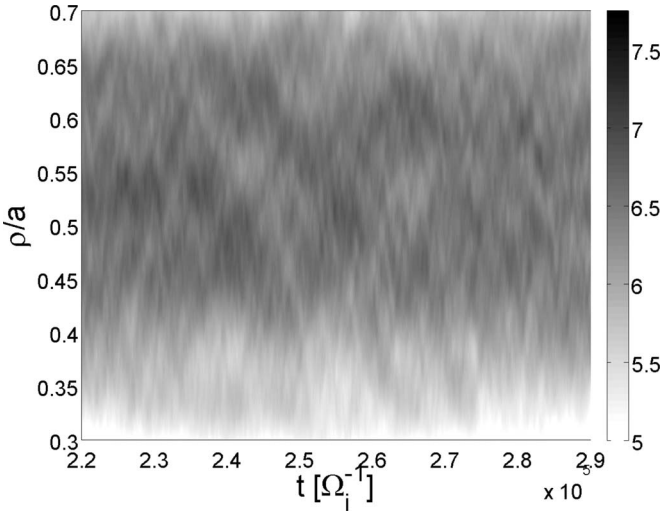

FIG. 11. Radial and temporal profiles of R_0/L_{Ti} at the end of heated simulation.

fast noise oscillations. This shows that quasisteady states obtained with PIC codes not only manifest incorrect transport (in the average sense) but also incorrect qualitative physics. On the other hand, simulations that reach a steady state demonstrate the true time evolution due to turbulent physics. The difference is more clear in Figs. 11 and 12, which show the radial and temporal evolutions of R_0/L_{Ti}. In the noise-controlled-heated case, inward propagating avalanches of temperature bursts are clearly visible. When the noise control algorithm is turned off, these bursts disappear and the amplitude of temperature gradient fluctuations becomes smaller. This is the manifestation of the filamentation of the velocity phase space. At the best of our knowledge the bursty behavior observed in noise-controlled-heated simulations is not specific to the way the plasma is heated. Several different cases have been run including large systems without any heating where the plasma temperature decays sufficiently slowly to have a long enough time with the temperature gra-

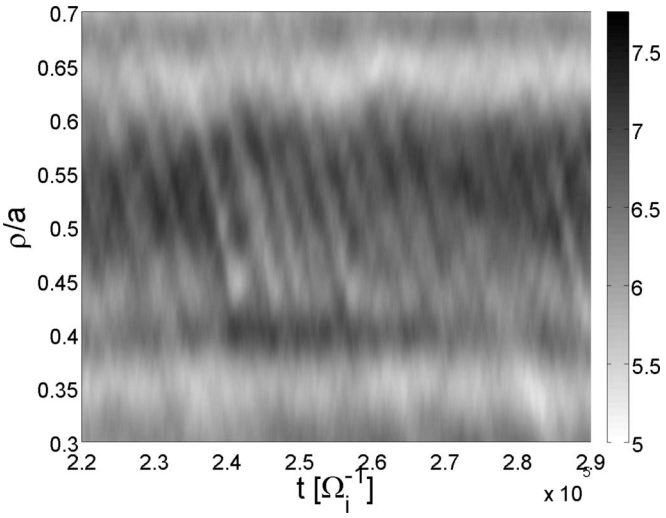

FIG. 12. Radial and temporal profiles of R_0/L_{Ti} at the end of noise-controlled-heated simulation.

TABLE I. Summary of heat diffusivity and normalized temperature gradient. Values in brackets indicate unconverged results. The noise-controlled-fixed-gradient case has been run with 4×80 M=320 M markers.

Simulation	Steady state	Heated	$\langle\chi_i/\chi_{GB}\rangle$	±	$\langle R_0/L_{Ti}\rangle$	±
Transient	No	No	(0.30)	(0.03)	(5.38)	(0.05)
Noise-controlled	Yes	No	0.13	0.11	5.83	0.10
Noise-controlled-fixed-gradient	Yes	Yes	0.63	0.18	6.68	0.09
Heated	No	Yes	(1.06)	(0.12)	(6.52)	(0.05)
Noise-controlled-heated	Yes	Yes	0.93	0.29	6.52	0.11

dient well above marginal and in which a similar bursty behavior is observed. A more detailed analysis of bursts and avalanche behavior is presented in Ref. 53.

Note that the fluctuation entropy also provides an additional way to check the numerical convergence of the simulation. The fluctuation entropy diagnostic is unambiguously defined in contrast to signal to noise diagnostic: The latter is obtained by manually defining which modes belong to the noise and which modes belong to the signal and depends on the field-aligned filter. The criterion of a signal to noise ratio higher than 10 is of course empirical only because it depends itself on the definition of noise and is based on experience. The fluctuation entropy diagnostic has the advantage that it does not rely on any assumption. It is in fact strongly connected to the sum of the weights squared and has in addition a physical interpretation (as seen above, D_{flux} connects to the heat diffusivity, D_{field} connects to the energy transfer between the field and particles, and D_{nc} connects to the dissipation artificially introduced in the system). It is therefore an extremely useful tool for gyrokinetic PIC simulations. However, future work is needed to quantify the "steadiness" of the final state of a simulation. At this stage, the fluctuation entropy has only been studied qualitatively and does not provide a quantitative criterion in contrast to the signal to noise ratio such that both diagnostics must be used. All these issues are left for further studies.

D. Summary

Table I gives a summary of the five simulations done in this work by showing the heat diffusivity χ_i/χ_{GB}, where $\chi_{GB}=\rho_s^2 c_s/a$ is the gyrobohm normalization and the normalized temperature gradient R_0/L_{Ti}. All physical quantities have been spatially averaged between $\tilde{\rho}=0.4$ and $\tilde{\rho}=0.6$. For the transient case, the time average is done in the end of the nonlinear phase between $t_1=541a/c_s$ and $t_2=812a/c_s$. For all other simulations, the time average is done between t_1 and $t_3=1570a/c_s$. The noise-controlled case has been rerun with 320M markers such that the signal to noise ratio is close to but above 10. The error is the standard deviation of the spatially averaged signal. Nonconverged results (in terms of signal to noise ratio) are put inside brackets. From Table I, one sees that the transient case is not converged: This is reflected in the value of R_0/L_{Ti} which is well below the nonlinear critical gradient of $R_0/L_{Ti}=6$.[7] In the later part of the simulation, the gradient appears to decrease indefinitely below the critical value and is interpreted as the result of noise accumulation. The *noise-controlled-fixed-gradient* and noise-controlled-heated cases differ only by heating algorithms, i.e., by the difference between $S_K(\vec{z},t)+S_{\text{corr}}(\vec{z},t)$ and $S_H(\vec{z},t)$. The influence of the heating algorithm on heat transport is left for future works. Finally, one sees that the heated simulation gives good quantitative values compared to the noise-controlled-heated case although it is completely dominated by noise. As seen from Sec. IV C, the avalanche process is completely suppressed, therefore the good quantitative agreement must be considered as purely coincidental.

V. CONCLUSION

In this work, the notion of steady state has been studied with the help of the fluctuation entropy evolution equation using the global collisionless PIC code ORB5. The well-known result that δf collisionless PIC simulations cannot reach a true steady state in the absence of dissipation has been recovered. It was then shown that the noise-control algorithm allows these simulations to reach a steady state, proving that the W-stat proposed in Ref. 32 is able to resolve the entropy paradox for a global 5D collisionless PIC code. Two categories of simulations have been studied. In decaying simulations, as the system evolves toward the marginal point, it becomes more and more difficult to describe accurately the perturbed distribution function with the markers such that the noise will sooner or later become too large. The signal to noise ratio and the fluctuation entropy diagnostics determine for a given particle number and a given value of artificial dissipation how close to the marginal point the simulation will remain well converged. In driven simulations, the steady state can *a priori* be maintained indefinitely provided that the noise-control algorithm is turned on: The system remains far from the marginal point which keeps the signal high. However, when the noise-control algorithm is not used, the heating algorithm (designed in a way that does not act on the phase space filamentation) alone does not allow a steady state. Even worse, the noise accumulation suppresses the avalanche process. Therefore, this work shows that the noise issue, which is most of the time discussed for ETG turbulence, must not be neglected for ITG turbulence either. In this respect, the entropy diagnostic is very simple to implement and is an extremely powerful tool.

Finally, it is worth commenting the coarse-graining method[38] which, by suppressing the phase space filamentation, is by nature also a noise-control algorithm. The coarse-graining method is computationally more expensive but it preferentially suppresses the small scales, whereas the noise-control algorithm described here does not make any distinc-

tion of scales. Therefore, a comparison of these two schemes, together with the Eulerian approach, would be desirable in order to understand the effects of numerical dissipation on plasma turbulence simulations.

ACKNOWLEDGMENTS

All simulations have been run on the IBM Blue Gene/L parallel machine at the Ecole Polytechnique Fédérale de Lausanne. This work has been partly supported by the Swiss National Science Foundation.

APPENDIX: NEGATIVITY OF D_{nc} AND D_{heat}

First, the proof that $D_{nc} \leq 0$ is given. It is easier to work with the discretized form of D_{nc}. δf is discretized with the usual Klimontovitch distribution. One finds

$$D_{nc} = \sum_{k=1}^{N_S} \sum_{p=1}^{N_k} -\gamma_K \frac{\tilde{w}_p^2}{\tilde{f}_{0p}} + \tilde{w}_p \sum_{j=1}^{N_{mom}} g_j^k M_j(\vec{z}_p). \tag{A1}$$

One has $\tilde{w}_p = w_p \Omega_p$ and $\tilde{f}_{0p} = f_0(\vec{z}_p)\Omega_p$, where w_p (respectively Ω_p) is the weight (respectively the phase space volume) of the marker p. The Krook operator is discretized on N_S equidistant bins. For each bin k containing N_k markers, g_j^k is obtained through the linear system

$$\sum_{p=1}^{N_k} \tilde{w}_p \gamma_K M_j(\vec{z}_p) = \sum_{p=1}^{N_k} \sum_{i=1}^{N_{mom}} \tilde{f}_{0p} M_i(\vec{z}_p) M_j(\vec{z}_p) g_i^k. \tag{A2}$$

Multiplying this equation by g_j^k, summing over j, and inserting the result in Eq. (A1), one gets $D_{nc} = \Sigma_k D_{nc}^k$ with

$$D_{nc}^k = \sum_{p=1}^{N_k} \frac{1}{\gamma_K \tilde{f}_{0p}} \left\{ -(\gamma_K \tilde{w}_p)^2 + \left[\sum_{i=1}^{N_{mom}} \tilde{f}_{0p} g_i^k M_i(\vec{z}_p) \right]^2 \right\}. \tag{A3}$$

Therefore D_{nc}^k can be positive if for at least one marker the following identity is satisfied,

$$|\gamma_K \tilde{w}_p| < \sum_{i=1}^{N_{mom}} |\tilde{f}_{0p} g_i^k M_i(\vec{z}_p)|. \tag{A4}$$

It means that for this marker the contribution of $S_K(\vec{z},t)$ is smaller than the contribution of $S_{corr}(\vec{z},t)$. This is of course not possible as $S_{corr}(\vec{z},t)$ is a projection of $S_K(\vec{z},t)$ over a finite number of velocity moments. In extreme cases where the number of markers per bin is of the order unity, D_{nc} could be positive, but in practice this never happens as N_S is typically equal to $1/\rho^*$, which is obviously much smaller than the total number of markers. The same arguments can be used to show that D_{heat} is always negative.

[1] X. Garbet, Plasma Phys. Controlled Fusion **43**, A251 (2001).
[2] Z. Lin, T. S. Hahm, W. W. Lee, W. M. Tang, and R. B. White, Science **281**, 1835 (1998).
[3] J. E. Kinsey, G. M. Staebler, and R. E. Waltz, Phys. Plasmas **15**, 055908 (2008).
[4] C. Angioni, L. Carraro, N. Dubuit, R. Dux, C. Fuchs, X. Garbet, L. Garzotti, C. Giroud, R. Guirlet, F. Jenko, O. J. W. F. Kardaun, L. Lauro-Taroni, P. Mantica, M. Maslov, V. Naulin, R. Neu, A. G. Peeters, G. Pereverzev, M. E. Puiatti, T. Pütterich, J. Stober, M. Valovic, M. Valisa, H. Weisen, A. Zabolotsky, the Asdex Upgrade Team, and JET EFDA Contributors, Phys. Plasmas **14**, 055905 (2007).
[5] J. Candy and R. Waltz, Phys. Rev. Lett. **91**, 045001 (2003).
[6] M. N. Rosenbluth and F. L. Hinton, Phys. Rev. Lett. **80**, 724 (1998).
[7] A. M. Dimits, G. Bateman, M. A. Beer, B. I. Cohen, W. Dorland, G. W. Hammett, C. Kim, J. E. Kinsey, M. Kotschenreuter, A. H. Kritz, L. L. Lao, J. Mandrekas, W. M. Nevins, S. E. Parker, A. J. Redd, D. E. Shumaker, R. D. Sydora, and J. Weiland, Phys. Plasmas **7**, 969 (2000).
[8] G. Rewoldt, Z. Lin, and Y. Idomura, Comput. Phys. Commun. **177**, 775 (2007).
[9] G. L. Falchetto, B. D. Scott, P. Angelino, A. Bottino, T. Dannert, V. Grandgirard, S. Janhunen, F. Jenko, S. Jolliet, A. Kendl, B. F. McMillan, V. Naulin, A. H. Nielsen, M. Ottaviani, A. G. Peeters, M. J. Pueschel, D. Reiser, T. Ribeiro, and M. Romanelli, Plasma Phys. Controlled Fusion **50**, 124015 (2008).
[10] F. Jenko, W. Dorland, M. Kotschenreuter, and B. N. Rogers, Phys. Plasmas **7**, 1904 (2000).
[11] Z. Lin, L. Chen, and F. Zonca, Phys. Plasmas **12**, 056125 (2005).
[12] L. Villard, P. Angelino, A. Bottino, S. J. Allfrey, R. Hatzky, Y. Idomura, O. Sauter, and T. M. Tran, Plasma Phys. Controlled Fusion **46**, B51 (2004).
[13] J. Candy, R. E. Waltz, S. E. Parker, and Y. Chen, Phys. Plasmas **13**, 074501 (2006).
[14] T. Dannert and F. Jenko, Phys. Plasmas **12**, 072309 (2005).
[15] J. Lang, S. E. Parker, and Y. Chen, Phys. Plasmas **15**, 055907 (2008).
[16] J. Candy and R. Waltz, J. Comput. Phys. **186**, 545 (2003).
[17] F. Jenko, Comput. Phys. Commun. **125**, 196 (2000).
[18] Y. Idomura, M. Ida, and S. Tokuda, Phys. Plasmas **13**, 227 (2008).
[19] M. Kotschenreuther, G. Rewoldt, and W. M. Tang, Comput. Phys. Commun. **88**, 128 (1995).
[20] B. D. Scott, Plasma Phys. Controlled Fusion **39**, 1635 (1997).
[21] C. Z. Cheng and G. Knorr, J. Comput. Phys. **22**, 330 (1976).
[22] M. Brunetti, V. Grandgirard, O. Sauter, J. Vaclavik, and L. Villard, Comput. Phys. Commun. **163**, 1 (2004).
[23] V. Grandgirard, M. Brunetti, P. Bertrand, N. Besse, X. Garbet, P. Gendrih, G. Manfredi, Y. Sarazin, O. Sauter, E. Sonnendrucker, J. Vaclavik, and L. Villard, J. Comput. Phys. **217**, 395 (2006).
[24] V. Grandgirard, Y. Sarazin, P. Angelino, A. Bottino, N. Crouseilles, G. Darmet, G. Dif-Pradalier, X. Garbet, P. Ghendrih, S. Jolliet, G. Latu, E. Sonnendrucker, and L. Villard, Plasma Phys. Controlled Fusion **49**, B173 (2007).
[25] W. W. Lee, Phys. Fluids **26**, 256 (1983).
[26] T. M. Tran, K. Appert, M. Fivaz, G. Jost, J. Vaclavik, and L. Villard, in *Theory of Fusion Plasmas*, edited by E. Compositori (Societá Italiana di Fisica, Bologna, 1999), p. 45.
[27] S. E. Parker, C. Kim, and Y. Chen, Phys. Plasmas **6**, 1709 (1999).
[28] A. M. Dimits, T. J. Williams, J. A. Byers, and B. I. Cohen, Phys. Rev. Lett. **77**, 71 (1996).
[29] R. D. Sydora, V. C. Decyck, and J. M. Dawson, Plasma Phys. Controlled Fusion **38**, A281 (1996).
[30] Y. Idomura, Nucl. Fusion **43**, 234 (2003).
[31] W. M. Nevins, S. E. Parker, Y. Chen, J. Candy, A. Dimits, W. Dorland, G. W. Hammett, and F. Jenko, Phys. Plasmas **14**, 084501 (2007).
[32] J. A. Krommes, Phys. Plasmas **6**, 1477 (1999).
[33] J. L. V. Lewandowski, Phys. Plasmas **12**, 052322 (2005).
[34] Y. Chen and R. B. White, Phys. Plasmas **4**, 3591 (1997).
[35] S. Brunner, E. Valeo, and J. A. Krommes, Phys. Plasmas **6**, 4504 (1999).
[36] J. Denavit, J. Comput. Phys. **9**, 75 (1972).
[37] S. Vadlamani, S. E. Parker, Y. Chen, and C. Kim, Comput. Phys. Commun. **164**, 209 (2004).
[38] Y. Chen and S. E. Parker, Phys. Plasmas **14**, 082301 (2007).
[39] B. F. McMillan, S. Jolliet, T. M. Tran, L. Villard, A. Bottino, and P. Angelino, Phys. Plasmas **15**, 052308 (2008).
[40] S. Jolliet, A. Bottino, P. Angelino, R. Hatzky, T. M. Tran, B. F. McMillan, O. Sauter, K. Appert, Y. Idomura, and L. Villard, Comput. Phys. Commun. **177**, 409 (2007).
[41] T. Hahm, Phys. Fluids **31**, 2670 (1988).
[42] P. Angelino, A. Bottino, R. Hatzky, S. Jolliet, O. Sauter, T. M. Tran, and L. Villard, Phys. Plasmas **13**, 052304 (2006).
[43] A. Y. Aydemir, Phys. Plasmas **1**, 822 (1994).
[44] M. Fivaz, S. Brunner, G. de Ridder, O. Sauter, T. M. Tran, J. Vaclavik, L. Villard, and K. Appert, Comput. Phys. Commun. **111**, 27 (1998).
[45] A. Bottino, A. G. Peeters, R. Hatzky, S. Jolliet, B. F. McMillan, T. M. Tran, and L. Villard, Phys. Plasmas **14**, 010701 (2007).

[46]R. Hatzky, T. M. Tran, A. Koenies, R. Kleiber, and S. J. Allfrey, Phys. Plasmas **9**, 898 (2002).
[47]T.-H. Watanabe and H. Sugama, Phys. Plasmas **9**, 3659 (2002).
[48]X. Garbet, N. Dubuit, E. Asp, Y. Sarazin, C. Bourdelle, P. Gendrih, and G. T. Hoang, Phys. Plasmas **12**, 082511 (2005).
[49]H. Sugama and M. Okamoto, Phys. Plasmas **3**, 2379 (1996).
[50]T.-H. Watanabe and H. Sugama, Phys. Plasmas **11**, 1476 (2004).
[51]J. Candy and R. E. Waltz, Phys. Plasmas **13**, 032310 (2006).
[52]Y. Idomura, M. Ida, S. Tokuda, and L. Villard, J. Comput. Phys. **226**, 244 (2007).
[53]B. F. McMillan, S. Jolliet, T. M. Tran, L. Vilard, A. Bottino, and P. Angelino, Phys. Plasmas **16**, 022310 (2009).